
Termodinámica

Revista Mexicana de Ingeniería Química

Vol. 14, No. 1 (2015) 213-229

THERMOPHYSICAL PROPERTIES OF R744 IN SUPERCRITICAL REGION DURING THE STARTUP OF GAS COOLING PROCESS

PROPIEDADES TERMOFÍSICAS DEL R744 EN LA REGIÓN SUPERCRÍTICA DURANTE EL PROCESO DEL ARRANQUE DEL GAS COOLER

J.F. Ituna-Yudonago and J.M. Belman-Flores*

Department of Mechanical Engineering, Engineering Division, Campus Irapuato-Salamanca, University of Guanajuato, Salamanca, Gto., Mexico.

Received April 19, 2014; Accepted february 23, 2015

Abstract

In this paper, the thermophysical properties of carbon dioxide (R744) in supercritical region during the startup of gas cooling process were widely investigated in a horizontal hairpin gas cooler. The dynamic model was discretized by the fully implicit finite volume method. The thermophysical properties were evaluated through the REFPROP dynamic libraries linked to Matlab. The results showed that, the thermophysical properties of R744 are characterized by large variations along the gas cooler during the transient period. In the pseudo-critical region, the behavior of the specific heat, thermal conductivity, density and dynamic viscosity is characterized by an instantaneous change in the amplitude. The specific heat is the property most affected by the transient phenomenon in the gas cooler. Its behavior has a great impact on the local heat transfer coefficient of R744.

Keywords: gas cooler, carbon dioxide, thermophysical properties, transient phenomenon, transcritical system.

Resumen

En este trabajo, se investigan ampliamente las propiedades termofísicas del dióxido de carbono (R744) en la región supercrítica durante el arranque del proceso de enfriamiento de gas, en un enfriador horizontal de tipo horquilla. El modelo dinámico fue discretizado mediante el método de volúmenes finitos completamente implícito. Las propiedades termofísicas se evaluaron a través de las bibliotecas dinámicas REFPROP vinculadas a Matlab. Los resultados mostraron que, las propiedades termofísicas del R744 se caracterizan por grandes variaciones a lo largo del enfriador de gas durante el período transitorio. En la región pseudo-crítica, el comportamiento del calor específico, conductividad térmica, densidad y viscosidad dinámica se caracteriza por un cambio instantáneo en la amplitud. El calor específico es la propiedad más afectada por el fenómeno transitorio en el enfriador de gas. Su comportamiento tiene un gran impacto en el coeficiente de transferencia de calor local del R744.

Palabras clave: enfriador de gas, dióxido de carbono, propiedades termofísicas, fenómeno transitorio, sistema transcrítico.

1 Introduction

Vapor compression system, is the most widely used technology for refrigeration and air conditioning. Its popularity is due to its high coefficient of performance (COP), compactness, and lower operating costs. Despite these advantages, the main drawbacks of vapor compression systems are the high energy consumption and the leakage of refrigerants, belonging to chlorofluorocarbons (CFCs), hydrochlorofluorocarbons (HCFCs) which have greater Ozone Depletion Potential (ODP) and Global Warming Potential (GWP) (Lugo-Leyte *et al*., 2013; Belman-Flores *et al*., 2014). So, faced with this precarious situation and according to the Kyoto (Woerdman, 2000) and Montreal protocol (Dull *et al*., 1989), scientists began to look for new alternatives. However, several studies have focused on the use of refrigerants which belong to the family of hydrocarbons (Granryd, 2001), hydrofluoroolefins

*Corresponding author. E-mail: : jfbelman@ugto.mx

(Tanaka and Higashi, 2010), blends (Neil and Owen, 2004), and natural refrigerants (Bolaji and Huan, 2013) in which there are: carbon dioxide (ASHRAE, 2009), ammonia (Björn, 2008), water (Lachner, 2007) and air (Butler *et al*., 2001). Unlike all these new alternatives, carbon dioxide has a remarkable advantage because it is nontoxic, nonflammable, and no harmful environmental impact. Despite the advantages offered by the carbon dioxide, its main inconveniences are the low critical temperature (31.06 °C) and the high critical pressure (7.38 MPa). With a lower critical temperature, the vapor compression system operating with the R744 tends to have a higher volumetric capacity for a given application; therefore, leads to a decrease in the COP (Sarkar and Agrawal, 2010). Furthermore, the high critical pressure causes several effects that influence in the design of the components, particularly the design of compressors and heat exchangers. Also, it can create security problems in the cycle components (Kim *et al*., 2004). It should be noted that the vapor compression system operating with carbon dioxide in transcritical conditions is most concerned by the instability in the thermophysical properties. This instability occurs more in the supercritical region, and precisely in the heat exchanger called gas cooler. In this heat exchanger, a little variation in temperature or pressure can produce a large change in the thermophysical properties, and then leads to significant variations in both heat transfer and fluid flow behaviors. These variations are more meaningful when the R744 temperature is near the critical point (Peixue *et al*., 2008; Sánchez *et al*., 2012).

In this way, several investigations on the behavior of the thermophysical properties of R744, the heat transfer coefficient and pressure drop during gas cooling process began to be conducted on different types of gas cooler such as: horizontal single in-tube (Son and Park, 2006), horizontal macro, mini or micro channels (Huai *et al*., 2005; Yun *et al*., 2007), vertical multi-port tube or mini-channels (Liao and Zhao, 2002; Duffey and Pioro, 2005; Yoon-Yeong and Hwan-Yeol, 2009). Other works have been focused on bundles and finned tubes technology (Zhao and Ohadi, 2004; Ge and Cropper, 2009). In general, these studies were focused on the impacts of variations in the operating pressure and/or mass flow of R744, as well as in the diameter of tube wherein the R744 flows, on the heat transfer coefficient and pressure drop. Son and Park (2006) investigated on heat transfer and pressure drop characteristics of R744 during gas cooling process in a horizontal tube. Results of this study showed that the local heat transfer coefficient decreases when the gas cooling pressure increases during the process. However, in the middle stage of gas cooling process where the refrigerant temperature is close to the critical temperature, the heat transfer coefficient changes much with respect to the pressure variation. But, for constant inlet pressure of gas cooler, the local heat transfer coefficient increases with respect to the mass flux. Similar results were also obtained by Liao and Zhao (2002). As emphasized by Huai *et al*., (2005), the mass flux has a significant influence on the pressure drop at a fixed operating pressure, the pressure drop increases with the mass flux. But, for a fixed mass flux, the pressure drop decreases with the operating pressure because the variation in the thermophysical properties of R744 becomes smaller as the operating pressure increases.

Some research (Kim *et al*., 2007; Dang and Hihara, 2010; Hoo-Kyu and Chang-Hyo, 2010; Li *et al*., 2011; Fang and Xu, 2011) have focused in the development of new correlations to calculate heat transfer coefficient, given that there were some inconsistencies between theoretical results based on some existing correlations and experimental results. Others have addressed the dynamic analysis of gas cooler. These studies were specially carried out on the steady state behaviors of thermophysical properties and heat transfer coefficient. Sánchez *et al*., (2012) developed and validated a stationary model of a water-R744 coaxial gas cooler. This model based on the finite volume method, was designed to analyze the effect of the number of finite volume on the maximum error of the enthalpy and heat capacity of the gas cooler, and the influence of the variables that determine the gas cooler thermal effectiveness. Despite the interesting results obtained in steady state, no information about the transient state of the analyzed properties has been given. Ge and Cropper (2009) used the distributed method for developing the steady state model of finned-tube air-cooled R744 gas cooler, in order to predict accurately the great variation of both refrigerant thermophysical properties and local heat transfer coefficients during R744 gas cooling process. The model has been validated with the test results from published literature by comparing the gas temperature profiles along the coil pipes from inlet to outlet at different operating conditions. Results showed that the temperature and the heat capacity are both improved with the increase of heat exchanger circuit numbers. Peixue *et al*., (2008) investigated on the method to obtain the local heat transfer coefficients of carbon dioxide at supercritical pressures in vertical

multi-port mini-channels and in a vertical small tube under cooling process. Steady state behavior of heat transfer coefficient along the gas cooler was carefully analyzed. The experimental results showed that the sharply variable thermophysical properties of carbon dioxide have a significant effect on the local heat transfer coefficient which varies significantly along the vertical mini-channels and small tube when the R744 bulk temperatures were near the critical region.

By analyzing the contents of different work referenced above, it becomes clear that there is no work in which behaviors of all thermophysical properties are widely described. Most of analyses are limited in describing the behavior of properties or heat transfer coefficient depending on the temperature of R744, in order to know how they behave with respect to the critical or pseudo-critical temperature, without showing how each property behaves along the gas cooler during the process. In addition, no research has focused on the analysis of the transient behavior of R744 properties, while it well known to all that transcritical systems are very sensitive to changes in operating conditions, and the gas cooler is the component in which temperature and pressure of the refrigerant are independent (Kim *et al*., 2004). This paper provides detailed information on the behavior of thermophysical properties of R744 during the gas cooling process, especially in transient regime. And also investigates on the impact of changes in these thermophysical properties on the local heat transfer coefficient during the transient period, with emphasis on the transient behavior of the Prandtl and Nusselt numbers, in order to have a better understanding of R744 behavior during the startup and steady operation of the gas cooler.

2 Description of the gas cooler

The gas cooler which is studied in this paper is a horizontal hairpin heat exchanger as shown in Fig. 1a. It is designed for an experimental facility which is under construction in the Engineering Division of the University of Guanajuato. This heat exchanger is constituted of nineteen inner tubes (see Fig. 1 b) in which the refrigerant (R744) flows. These tubes are assembled in an annulus (see Fig. 1c) causing a counter-flow arrangement with the secondary fluid (water). The characteristics of gas cooler are described in Table 1, where the material of each component is specified along with dimensions.

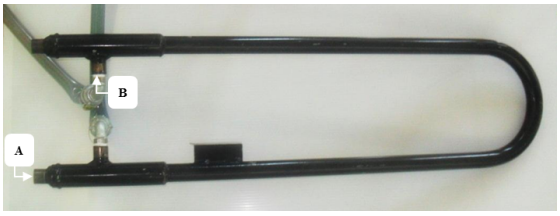

a) Top view of the gas cooler

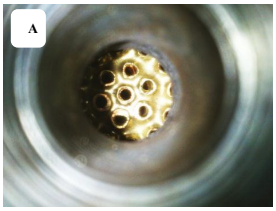

b) Inlet section of the refrigerant

c) Inlet section of the secondary fluid and profile view of the inner tubes

Fig. 1. Experimental gas cooler.

Table 1. Characteristics of the gas cooler.

Item	Material	Parameter	Magnitude
Inner tube	Stainless steel	Inner diameter (mm)	3.75
		Outer diameter (mm)	5.0
		Number of tubes	19
Annulus	Stainless steel	Inner diameter(mm)	30.0
		Outer diameter (mm)	33.7
		Radius of the bend (mm)	112.0
		Length (mm)	2000.0

3 Mathematical modeling

This section presents the mathematical formulation based on the mass, momentum, and energy conservation equations for both fluids circulating in the gas cooler. Each stream is discretized by the fully implicit finite volume method (FVM). The choice of this method is justified by the precision in the resulting solutions which are unconditionally stable in time and space over any group of control volumes and, of course, over the whole calculation domain (Patankar, 1980). This method is completed by the first order upwind differencing scheme for calculating fluxes through cell faces, because it enables the coefficients of the discretized equations being always positive, and therefore makes the solution physically realistic (Cariaga *et al*., 2013). In order to reduce the complexity in the analysis, some considerations are made as follows:

- Refrigerant and secondary fluid flows are modeled as a one-dimensional fluid flow.
- Axial heat conduction, viscous stress in fluid and heat radiation are negligible.
- The gas cooler is considered isolated. So all the heat removed from the refrigerant is transferred to the water.
- The cross sections of all inner tubes are constant

3.1 Refrigerant flow in the bare inner tube

The transient model of the refrigerant flow inside tubes is governed by the mass, momentum, and energy conservation equations. The first two equations are used to assess the velocity and pressure fields in the axial direction, while the third and fourth equations are used to evaluate the distribution of the enthalpy and wall temperature of the inner tube.

Mass conservation:

$$\frac{\partial(\rho \mathrm{A})_{\mathrm{r}}}{\partial \mathrm{t}} + \frac{\partial(\rho u \mathrm{A})_{\mathrm{r}}}{\partial \mathrm{z}} = 0 \tag{1}$$

Momentum conservation:

$$\frac{\mathrm{A_r}\partial(\rho \mathrm{u})_r}{\partial \mathrm{t}} + \frac{(\rho u \mathrm{A})_{\mathrm{r}}\partial u_r}{\partial \mathrm{z}} = -\frac{\mathrm{A_r}\partial P_r}{\partial \mathrm{z}} - \tau_z p_i \tag{2}$$

Energy conservation of refrigerant:

$$\frac{\partial(\rho \mathrm{Ah} - \mathrm{A}P)_r}{\partial \mathrm{t}} + \frac{\partial(\dot{m}h)_r}{\partial \mathrm{z}} = p_i \alpha_i (T_r - T_{ti}) \tag{3}$$

Wall energy conservation

$$\rho \mathrm{AC} p_{ti} \frac{\partial T_{ti}}{\partial \mathrm{t}} = p_i \alpha_i (T_r - T_{ti}) + p_o \alpha_o \left(T_{sf} - T_{ti}\right) \tag{4}$$

The discretization of these equations is performed by considering that each inner tube is divided into several control volumes as shown in Fig. 2a where P is the node of interest, W and E represent neighbor nodes to the west and east; w and e are the west and east faces of the control volume with u_W and u_e being their corresponding velocity. Furthermore, the boundary nodes are represented by A at the inlet and B at the outlet. This representation is designed for the discretization of the conservation equations of mass and energy, while the momentum equation which has the velocity as the main variable is discretized on the staggered control volumes as represented in Fig. 2b, where P^S, W^S and E^S are the staggered nodes with u_{w^S}, u_{P^S} and u_{e^S} their corresponding velocities. In addition, w^S and e^S are the west and east faces of the staggered control volume.

However, algebraic equations resulting from the discretization are presented in Eqs. (5-8). The first two algebraic equation systems (Eqs. 5-6) are used to determine the pressure and velocity fields by using the SIMPLE method (Patankar, 1980), while the two latter (Eqs. 7-8) are used to determine the refrigerant enthalpy and the wall temperature field. Thus, other thermophysical properties are calculated according to the pressure and enthalpy values in each node through the REFPROP dynamic libraries linked to Matlab (Lemmon *et al*., 2007). Details of this process are given in the global algorithm of resolution. Parameters by which the coefficients of each matrix are computed are described in Tables 2, 3, 4 and 5.

$$a_{P^S} u^*_{P^S} = a_{E^S} u^*_{E^S} + a_{W^S} u^*_{W^S} + b^*_{P^S} \tag{5}$$

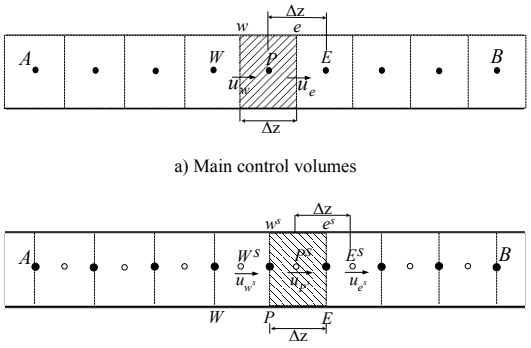

Fig. 2. Schematic representation of control volumes of the gas cooler.

Table 2. Coefficients of the algebraic equation of momentum conservation for refrigerant side.

Node	a_{P^s}	a_{W^s}	a_{E^s}	b_{P^s}
1	$max(-m_{r,A},0)+max(m^*_{r,e^s},0)$ $+\rho^*_{r,P^s}A_{r,P^s}\frac{\Delta z}{\Delta t}$	0	$max(m^*_{r,e^s},0)$	$\left[\rho^\circ_{r,P^s}u^\circ_{P^s}\frac{\Delta z}{\Delta t}+(P^*_P-P^*_E)\right]A_{r,p^s}$ $-\tau_z p_r \Delta z$
2,..., $(zn-1)$	$max(m^*_{r,w^s},0)+max(m^*_{r,e^s},0)$ $+\rho^\circ_{r,P^s}A_{r,P^s}\frac{\Delta z}{\Delta t}$	$max(m^*_{r,w^s},0)$	$max(m^*_{r,e^s},0)$	$\left[\rho^\circ_{r,P^s}u^\circ_{P^s}\frac{\Delta z}{\Delta t}+(P^*_P-P^*_E)\right]A_{r,p^s}$ $-\tau_z p_r \Delta z$
zn	$max(m^*_{r,w^s},0)+max(m^*_{r,e^s},0)$ $+\rho^\circ_{r,P^s}A_{r,P^s}\frac{\Delta z}{\Delta t}$	$max(m^*_{r,w^s},0)$	0	$\left[\rho^\circ_{r,P^s}u^\circ_{P^s}\frac{\Delta z}{\Delta t}+(P^*_W-P^*_P)\right]A_{r,p^s}$ $-\tau_z p_r \Delta z$

Table 3. Coefficients of the algebraic equation of pressure correction for refrigerant side.

Node	a^c_P	a^c_W	a^c_E	b^c_P
1	$\left(\frac{1}{c^2\Delta t}A_r\Delta z\right)_P+(\rho^* dA_r)_e$ $+\left(\frac{1}{2c^2}u^*A_r\right)_e$	0	$+(\rho^* dA_r)_e$ $+\left(\frac{1}{2c^2}u^*A_r\right)_e$	$(\rho^*u^*A_r)_A-(\rho^*u^*A_r)_e$ $+\left(\frac{1}{c^2\Delta t}A_r\Delta z\right)_P P'^\circ_P$
2,..., $(zn-1)$	$\left(\frac{1}{c^2\Delta t}A_r\Delta z\right)_P+(\rho^* dA_r)_e$ $+\left(\frac{1}{2c^2}u^*A_r\right)_e+(\rho^* dA_r)_w$ $-\left(\frac{1}{2c^2}u^*A_r\right)_w$	$+(\rho^* dA_r)_w$ $+\left(\frac{1}{2c^2}u^*A_r\right)_w$	$+(\rho^* dA_r)_e$ $+\left(\frac{1}{2c^2}u^*A_r\right)_e$	$(\rho^*u^*A_r)_w-(\rho^*u^*A_r)_e$ $+\left(\frac{1}{c^2\Delta t}A_r\Delta z\right)_P P'^\circ_P$
zn	$\left(\frac{1}{c^2\Delta t}A_r\Delta z\right)_P+(\rho^* dA_r)_e$ $+\left(\frac{1}{2c^2}u^*A_r\right)_e+(\rho^* dA_r)_w$ $-\left(\frac{1}{2c^2}u^*A_r\right)_w$	$+(\rho^* dA_r)_w$ $+\left(\frac{1}{2c^2}u^*A_r\right)_w$	0	$(\rho^*u^*A_r)_w-(\rho^*u^*A_r)_e$ $+\left(\frac{1}{c^2\Delta t}A_r\Delta z\right)_P P'^\circ_P$

$$a^c_P P'_P = a^c_E P'_E + a^c_W P'_W + b^c_P \tag{6}$$

$$a^{h_r}_P h_{r,P} = a^{h_r}_E h_{r,E} + a^{h_r}_W h_{r,W} + b^{h_r}_P \tag{7}$$

$$a^{T_{ti}}_P T_{tiP} = a^{T_{ti}}_E T_{tiE} + a^{T_{ti}}_W T_{tiW} + b^{T_{ti}}_P \tag{8}$$

Table 4. The coefficients of the algebraic equation of energy conservation for refrigerant side.

Node	$a_P^{h_r}$	$a_W^{h_r}$	$a_E^{h_r}$	$b_P^{h_r}$
1	$max\left[(-\dot{m}_r)_w,0\right]+max\left[(\dot{m}_r)_e,0\right]+\rho_P A_i\frac{\Delta z}{\Delta t}$	0	$max\left[-(\dot{m}_r)_w,0\right]$	$\left[\rho_P^\circ h_P^\circ+\left(P_P-P_P^\circ\right)\right]A_i\frac{\Delta z}{\Delta t}+p_i\alpha_i\left[T_{r,P}^\circ-T_{ti,P}^\circ\right]\Delta z+max\left[(\dot{m}_r)_w,0\right]h_A$
2,..., $(zn-1)$	$max\left[(-\dot{m}_r)_w,0\right]+max\left[(\dot{m}_r)_e,0\right]+\rho_P A_i\frac{\Delta z}{\Delta t}$	$max\left[(\dot{m}_r)_w,0\right]$	$max\left[-(\dot{m}_r)_e,0\right]$	$\left[\rho_P^\circ h_P^\circ+\left(P_P-P_P^\circ\right)\right]A_i\frac{\Delta z}{\Delta t}+p_i\alpha_i\left[T_{r,P}^\circ-T_{ti,P}^\circ\right]\Delta z$
zn	$max\left[(-\dot{m}_r)_w,0\right]+max\left[(\dot{m}_r)_e,0\right]+\rho_P A_i\frac{\Delta z}{\Delta t}$	$max\left[(\dot{m}_r)_w,0\right]$	0	$\left[\rho_P^\circ h_P^\circ+\left(P_P-P_P^\circ\right)\right]A_i\frac{\Delta z}{\Delta t}+p_i\alpha_i\left[T_{r,P}^\circ-T_{ti,P}^\circ\right]\Delta z$

Table 5. The coefficients of the algebraic equation of wall energy.

Node	$a_P^{T_{ti}}$	$a_W^{T_{ti}}$	$a_E^{T_{ti}}$	$b_P^{T_{ti}}$
1	$\frac{1}{\Delta t}\rho_{ti,P}^\circ A_r Cp_{ti,P}^\circ$	0	0	$p_i\alpha_i\left[T_{r,P}^\circ-T_{ti,P}^\circ\right]+p_o\alpha_o\left[T_{sf,P}^\circ-T_{ti,P}^\circ\right]+\frac{T_{ti,P}^\circ}{\Delta t}\rho_{ti,P}^\circ A_r Cp_{ti,P}^\circ$
2,..., $(zn-1)$	$\frac{1}{\Delta t}\rho_{ti,P}^\circ A_r Cp_{ti,P}^\circ$	0	0	$p_i\alpha_i\left[T_{r,P}^\circ-T_{ti,P}^\circ\right]+p_o\alpha_o\left[T_{sf,P}^\circ-T_{ti,P}^\circ\right]+\frac{T_{ti,P}^\circ}{\Delta t}\rho_{ti,P}^\circ A_r Cp_{ti,P}^\circ$
zn	$\frac{1}{\Delta t}\rho_{ti,P}^\circ A_r Cp_{ti,P}^\circ$	0	0	$p_i\alpha_i\left[T_{r,P}^\circ-T_{ti,P}^\circ\right]+p_o\alpha_o\left[T_{sf,P}^\circ-T_{ti,P}^\circ\right]+\frac{T_{ti,P}^\circ}{\Delta t}\rho_{ti,P}^\circ A_r Cp_{ti,P}^\circ$

3.2 Secondary fluid flow in the annulus

The mathematical formulation of secondary fluid flow in the annulus is similar to that presented for the refrigerant flow but, the only difference is that in this circuit, the pressure drops along the annular tube due to momentum change and the viscous friction are negligible. Therefore, the corresponding transient model is only governed by the energy conservation equation, which has the temperature of the secondary fluid as the main variable. The corresponding discretized model is presented in the following matrix system (Eq. 9), and the coefficients are described in Table 6.

$$a_P^{T_{sf}}T_{sf\,P}=a_E^{T_{sf}}T_{sf\,E}+a_W^{T_{sf}}T_{sf\,W}+b_P^{T_{sf}} \qquad (9)$$

Table 6. Coefficients of the discretized equation of energy for secondary fluid.

Node	$a_P^{T_{sf}}$	$a_W^{T_{sf}}$	$a_E^{T_{sf}}$	$b_P^{T_{sf}}$
1	$max\left[\left(-\dot{m}_{sf} Cp_{sf}\right)_A,0\right] + \left[\left(\dot{m}_{sf} Cp_{sf}\right)_e,0\right] + \left(\rho_{sf} Cp_{sf}\right)_P A_o \frac{\Delta z}{\Delta t}$	0	$max\left[-\left(\dot{m}_{sf} Cp_{sf}\right)_e,0\right]$	$\left[\rho^{\circ}_{sf,P} Cp^{\circ}_{sf,P} T^{\circ}_{sf,P} + \left(P_{sf,P} - P^{\circ}_{sf,P}\right)\right] A_o \frac{\Delta z}{\Delta t} + p_o \alpha_o \left[T^{\circ}_{ti,P} - T^{\circ}_{sf,P}\right] \Delta z + max\left[\left(\dot{m}_{sf} Cp_{sf}\right)_A,0\right] T_{sf,A}$
2,..., $(zn-1)$	$max\left[\left(-\dot{m}_{sf} Cp_{sf}\right)_w,0\right] + \left[\left(\dot{m}_{sf} Cp_{sf}\right)_e,0\right] + \left(\rho_{sf} Cp_{sf}\right)_P A_o \frac{\Delta z}{\Delta t}$	$max\left[\left(\dot{m}_{sf} Cp_{sf}\right)_w,0\right]$	$max\left[\left(-\dot{m}_{sf} Cp_{sf}\right)_e,0\right]$	$\left[\rho^{\circ}_{sf,P} Cp^{\circ}_{sf,P} T^{\circ}_{sf,P} + \left(P_{sf,P} - P^{\circ}_{sf,P}\right)\right] A_o \frac{\Delta z}{\Delta t} + p_o \alpha_o \left[T^{\circ}_{ti,P} - T^{\circ}_{sf,P}\right] \Delta z$
zn	$max\left[\left(-\dot{m}_{sf} Cp_{sf}\right)_w,0\right] + \left[\left(\dot{m}_{sf} Cp_{sf}\right)_e,0\right] + \left(\rho_{sf} Cp_{sf}\right)_P A_o \frac{\Delta z}{\Delta t}$	$max\left[\left(\dot{m}_{sf} Cp_{sf}\right)_w,0\right]$	0	$\left[\rho^{\circ}_{sf,P} Cp^{\circ}_{sf,P} T^{\circ}_{sf,P} + \left(P_{sf,P} - P^{\circ}_{sf,P}\right)\right] A_o \frac{\Delta z}{\Delta t} + p_o \alpha_o \left[T^{\circ}_{ti,P} - T^{\circ}_{sf,P}\right] \Delta z$

3.3 Boundary conditions

For the momentum equation, the inlet pressure is considered as boundary conditions, while for the energy equation, enthalpy from the compressor outlet is considered as inlet boundary conditions. In this study, no boundary condition at the exit of the gas cooler has been taken into account in order to let the model predicts the values of parameters at the gas cooler outlet. Data relating to boundary conditions were taken from the study realized by Pérez *et al*. (2013). Furthermore, in the annulus, the boundary conditions include the inlet water temperature, pressure and mass flow rate that correspond to the output operating conditions of the experimental heat dissipation system. For the inner tube, adiabatic boundary conditions are imposed at the lateral boundaries.

3.4 Heat transfer coefficient analysis

The behavior of the hairpin heat exchanger has attracted the attention of many researchers, due to the influence that has the radius of curvature on the heat transfer coefficient (Wojtkowiak and Popiel, 2000; Chen *et al*., 2004; Adam-Medina *et al*., 2013). The results of investigations performed on this heat exchanger have demonstrated that the friction factor is more influenced by the radius of curvature of the tube. However, new correlations have been developed by incorporating the radius of curvature as one of the parameters for calculating the friction factor (Chen *et al*., 2004). Unfortunately, these correlations were developed for refrigerants operating in subcritical conditions. Therefore, the lack of an appropriate correlation for the calculation of the friction factor in hairpin or return bend gas coolers has led some researchers to use correlations developed for straight in-tube gas coolers (Sánchez *et al*., 2012; Park and Hrnjak, 2007). Thus, in this study we use correlations developed for the straight in-tube gas coolers.

3.4.1 Inner heat transfer coefficient

Analysis of the heat transfer coefficient of R744 inside of inner tubes is calculated by using the Gnielinski (1976) correlation (Eq. 10) which was found by Rieberer (1999) to be the best for single-phase R744 at supercritical conditions. This correlation has presented interesting results in the study realized by Sánchez *et al*., (2012), with less than 10 % error in comparison with the correlation Pitla *et al*., (2002).

$$Nu_i = \frac{\left(\frac{f_i}{8}\right)\left(\mathrm{Re}_i - 1000\right)\mathrm{Pr}_i}{1 + 12.7\left(\frac{f_i}{8}\right)^{\frac{1}{2}}\left(\mathrm{Pr}_i^{\frac{2}{3}} - 1\right)} \tag{10}$$

$$0.5 < Pr_i < 2000; 2300 < \mathrm{Re}_i < 5 \times 10^5$$

$$\alpha_i = \frac{Nu_i k_r}{d_i} \tag{11}$$

The friction factor is calculated from Churchill (1977) correlation which extends over all flow regimes and all

relative roughness (δ):

$$f_i = 8\left\{\left(\frac{8}{\mathrm{Re}_i}\right)^{12} + \left[\left(2.457\ln\left(\frac{1}{\left(\frac{7}{\mathrm{Re}_i}\right)^{0.9} + 0.27\delta}\right)\right)^{16} + \left(\frac{37530}{\mathrm{Re}_i}\right)^{16}\right]^{\frac{-3}{2}}\right\}^{\frac{1}{12}} \tag{12}$$

3.4.2 Outer heat transfer coefficient

The outer heat transfer coefficient is obtained from the correlation developed by Petukhov *et al*., (1963) for water flowing in the secondary circuit (Eq.13), wherein geometric parameters such as tube length (L_t), inside diameter of annulus (D_i), hydraulic (D_h) and equivalent (D_{eq}) diameters are taken into account.

$$Nu_o = \frac{\left(\frac{f_o}{8}\right)\mathrm{Re}_o \cdot \mathrm{Pr}_o}{1 + 12.7\left(\frac{f_o}{8}\right)^{\frac{1}{2}}\left(\mathrm{Pr}_o^{\frac{2}{3}} - 1\right)} \cdot \left[1 + \left(\frac{D_h}{L_t}\right)^{\frac{2}{3}}\right] \cdot 0.86 \cdot \left(\frac{D_{eq}}{D_i}\right)^{-0.16} \tag{13}$$

$$\mathrm{Re}_i > 10^4$$

where $f_o = (1.8\log_{10}(\mathrm{Re}_o) - 1.5)^{-2}$

$$\alpha_o = \frac{Nu_o k_w}{D_\mathrm{h}} \tag{14}$$

3.5 Global algorithm of resolution

Fig. 3 shows the algorithm for simulating mathematical models of gas cooler. This methodology is subdivided into four steps: definition of input data, assessment of the pressure and velocity fields, resolution of the discretized energy equation, and the evaluation of R744 and water thermophysical properties. In the first step, geometrical parameters of the gas cooler, initial and boundary conditions are set. Once the data is provided to the program, the process passes to the second step which involves the calculation of the pressure and velocity fields of the refrigerant. After this step, pressure and velocity fields of both fluids are used to compute the dependent variables (enthalpy of R744, wall and water temperature). This computation is performed at each node and in several iterations until the convergence criteria is met. If the solution does not converge, then the process is reinitiated while adjusting the guessed pressure and velocity. But, if the convergence criteria are complied, one passes to the last step which is dedicated to the evaluation of thermophysical properties of R744, such as: specific heat, density, dynamic viscosity, thermal conductivity, as well as

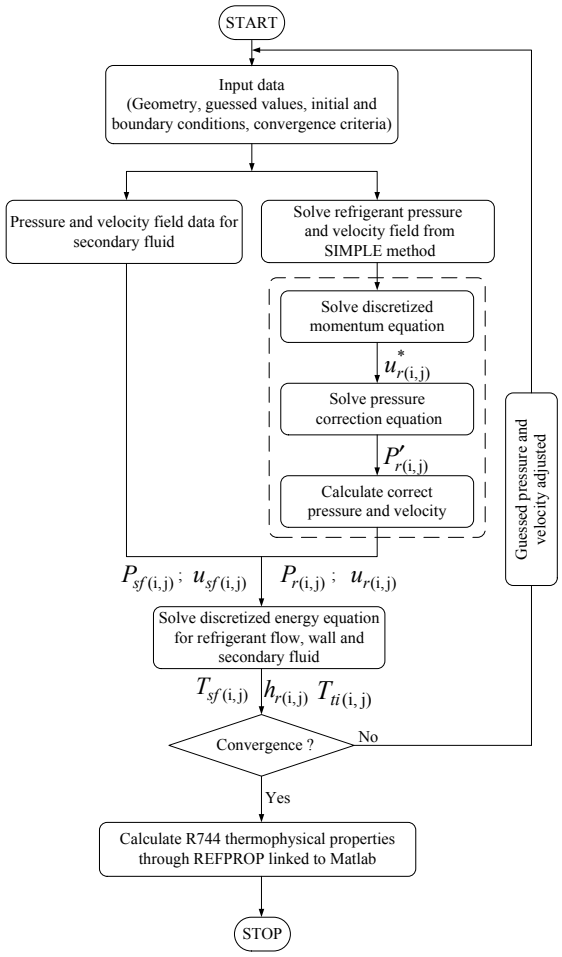

Fig. 3. Global algorithm of resolution.

Prandtl and Nusselt numbers and the heat transfer coefficient of R744. Thus, the process stops.

4 Results and discussion

This section presents the simulation results of the gas cooler dynamic model described previously. The simulation was performed by considering the average mass flux of R744 and water about 142.86 $\mathrm{kgm^{-2}s^{-1}}$ and 898.74 $\mathrm{kgm^{-2}s^{-1}}$, respectively. Results are presented graphically in space and time. With respect to space, twenty points of observation (namely twenty finite volumes with $\Delta z = 0.1$ m) are provided. These correspond to twenty points of temperature measurement planned in the experimental setup which is still in construction. While over time, a maximum of 240 seconds with $\Delta t = 0.5$s is provided which was supposed to be sufficient for observing the transient behavior of properties at startup.

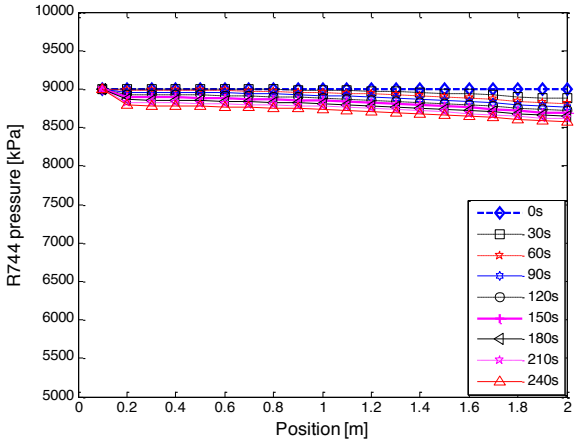

a) Pressure

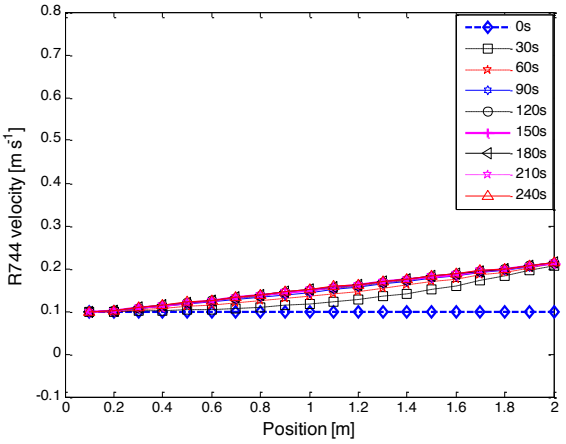

b) Velocity

Fig. 4. Distribution of pressure and velocity in the gas cooler.

Given the difficulty in reporting the results of all iterations, nine samples were selected in an interval of thirty seconds of observation. For a better understanding of transient phenomena that occur in each property, the results are graphically presented in three different forms. In the first type of graph, results of variations in each property depending on the position throughout the gas cooler during the first 240 seconds of gas cooling process are shown. This representation allows visualizing both transient and steady state of the property. In the second one, behavior of the property in each node of the finite volume (i.e. every 0.1 m of the gas cooler length) is shown, in order to identify the area that is affected the most by the transient effects. Finally, the third type of graph presents the effect of the R744 temperature on each property, this graph allows us to understand how each property behaves in the critical region. As mentioned in the previous section, before proceeding to the computation of thermophysical properties, an analysis of pressure, temperature and velocity fields is performed in order to know how these parameters are distributed along the gas cooler. Results of this analysis are shown in Fig. 4 where it can be observed the transient behaviors that occur in these parameters during startup of gas cooling process. Fig. 4a shows the pressure distribution in the gas cooler during the first 240 seconds of operation, where it can observed that there is no a significant change in pressure during the transitional period, but, the process is characterized by a decrease in pressure along the gas cooler which is estimated at 211 kPa between the inlet and outlet of the gas cooler. This pressure drop causes an increase in velocity (from 0.1 to 0.2 m s^{-1}) along the gas cooler as

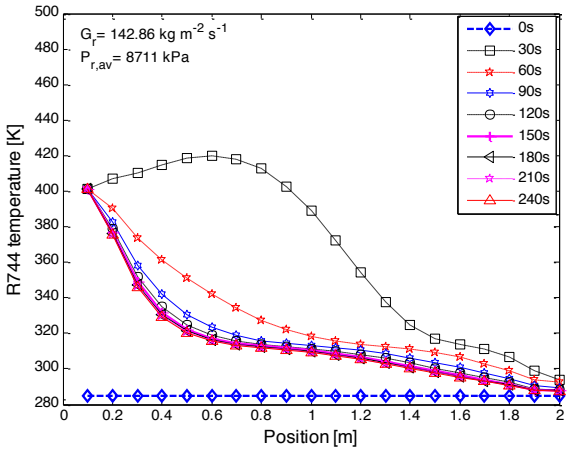

Fig. 5. Temperature distribution in the gas cooler.

seen in Fig. 4b. The average pressure of R744, ($P_{r,av}$) in the gas cooler is about 8711 kPa.

Temperature distribution of the refrigerant during the gas cooling process is shown in Fig. 5 where an important change is occurred in the 150 s before the temperature is stabilized. Instability in the first thirty seconds is much greater than in the rest of the startup period. In addition, the temperature undergoes a sharp drop between the inlet and 0.6 m in length. This change can have a significant influence on the behavior of thermophysical properties of the refrigerant as it operates in a supercritical area.

Transient behavior of the R744 thermophysical properties during the gas cooling process are shown in Fig. 6 where it can be observed the important change that occurs in each property during the first 150 seconds of the process. During this transient period, the profile of each sample undergoes a change

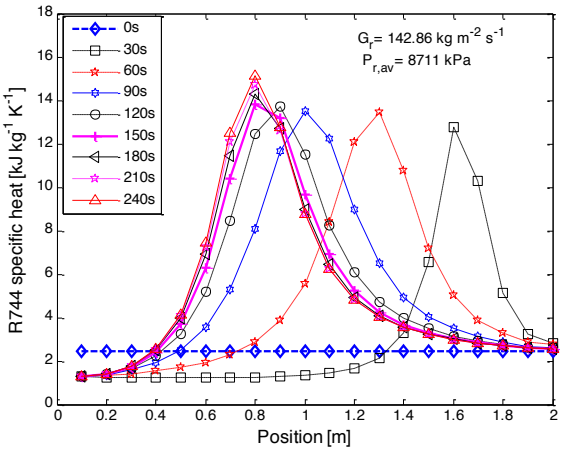

a) Specific heat vs position

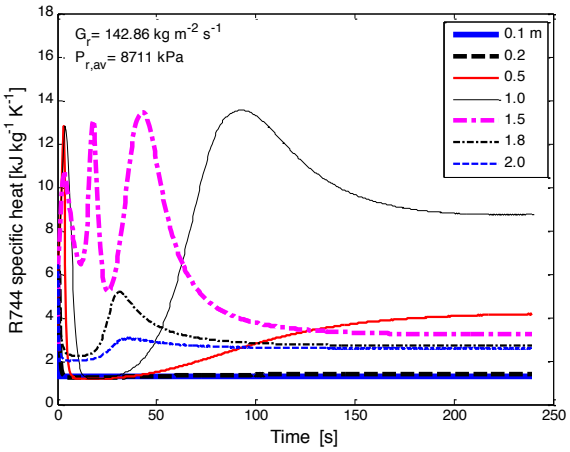

b) Specific heat vs time

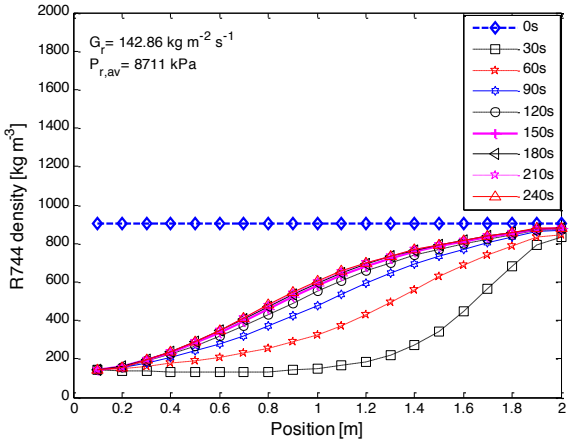

c) Density vs position

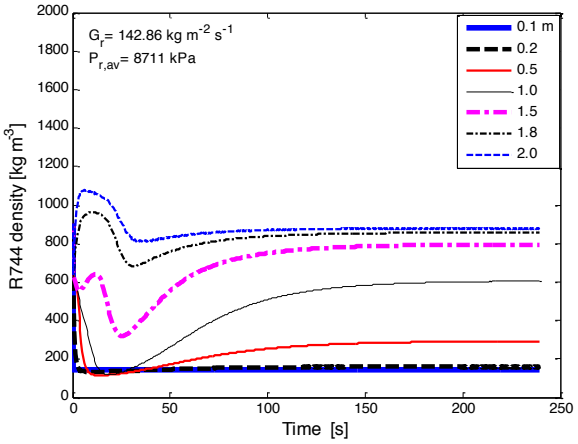

d) Density vs time

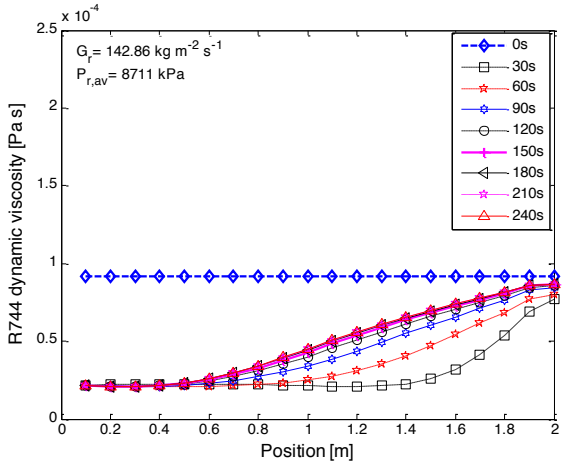

e) Dynamic viscosity vs position

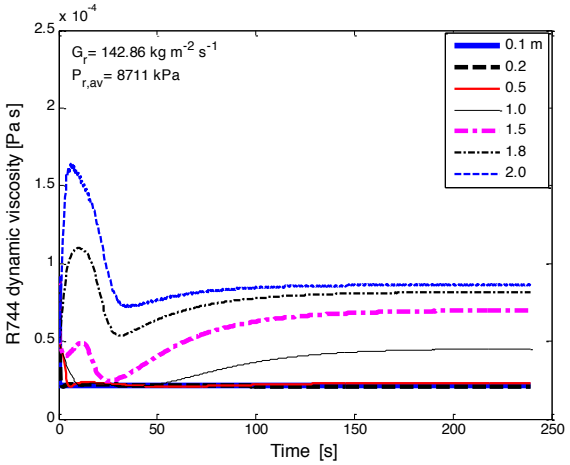

f) Dynamic viscosity vs time

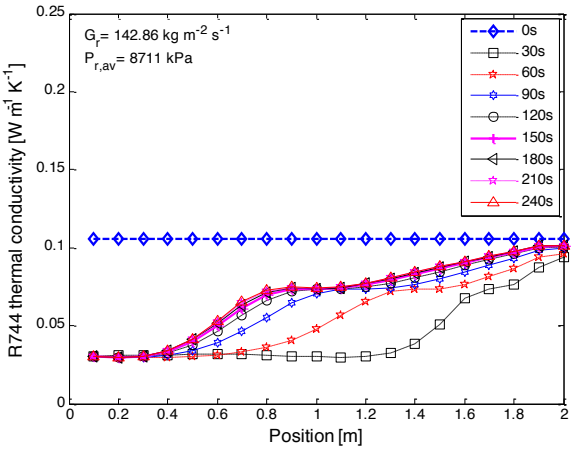

g) Thermal conductivity vs position

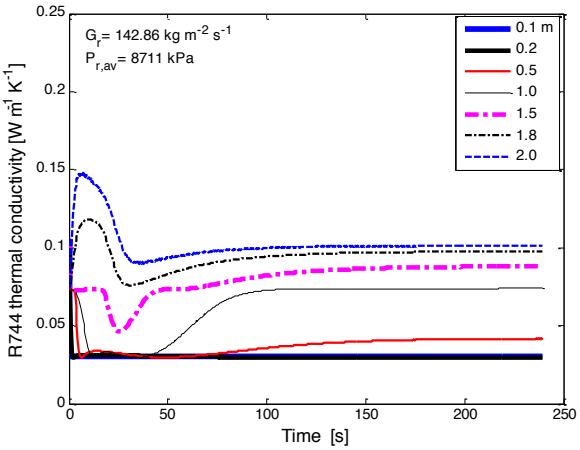

h) Thermal conductivity vs time

Fig. 6. Transient behavior of the R744 thermophysical properties along the gas cooler.

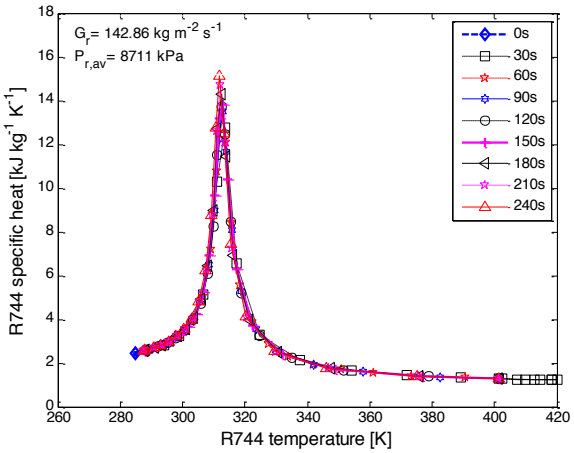

a) Specific heat

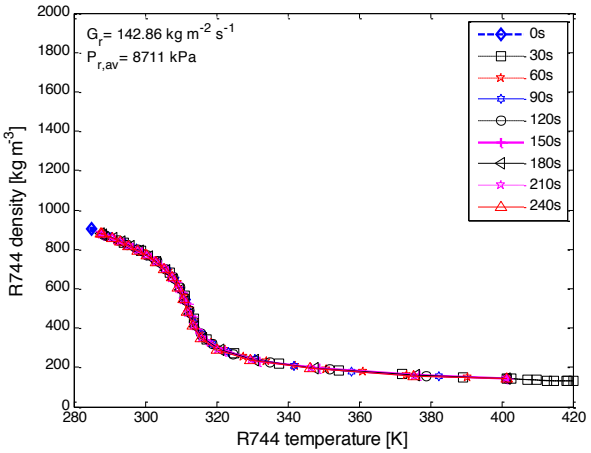

b) Density

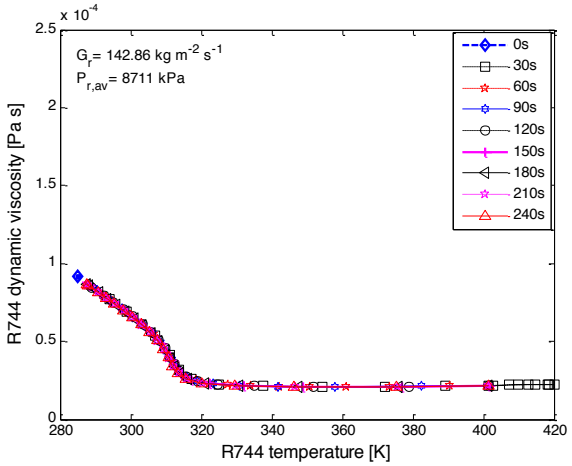

c) Dynamic viscosity

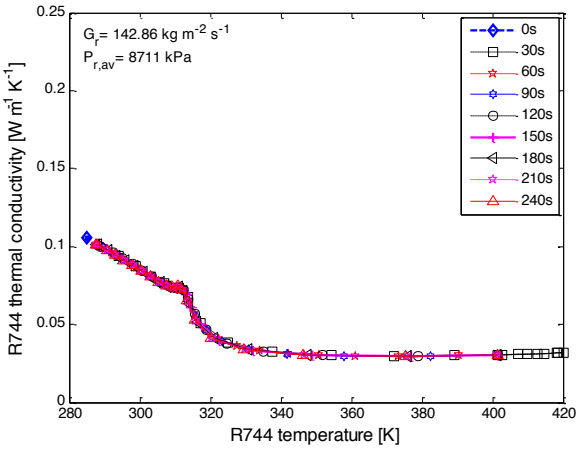

d) Thermal conductivity

Fig. 7. Transient behavior of the R744 thermophysical properties in the supercritical region.

in position along the gas cooler which leads to an increase in magnitude of each property. This transient effect is more pronounced in the specific heat which behaves differently in comparison with the other properties. The specific heat is characterized by an instantaneous change in the profile with a peak value that is 5 times higher than the ideal value (see Fig. 6a). By observing the profiles shown in Fig. 6b, it becomes clear that the transitional phenomenon of specific heat is more accentuated in the middle area of the gas cooler. Region in which the refrigerant flow undergoes a curvature of 180°. Therefore, the sudden and instantaneous change in the specific heat can have significant impacts on the performance of gas cooler, since this property is involved in the calculation of the heat transfer coefficient.

On the other hand, density, dynamic viscosity and thermal conductivity do not have significant transient phenomena during the process. Each property experienced a slight increase in magnitude along the gas cooler as shown in figs. 6c, 6e and 6g. Although transient effects in these properties are not very significant, they have anyway a fluctuation in the area near the exit of the gas cooler (see figs. 6d, 6f and 6h).

One of the important aspects of the analysis of thermophysical properties of R744 is to know how each property behaves in supercritical area. Fig. 7 presents the variation of each property depending on the local temperature of R744 while the mass flow and pressure are constant. It is evident from this analysis that, during the gas cooling process the thermophysical properties of R744 are closely related to its temperature. This interdependence is observed through the tendencies of sample profiles which are similar during the process. Fig. 7a shows a similar tendency to the presented in Fig. 6a, wherein the profile of the specific heat is characterized by a maximum value (about 7 times the nominal value) which occurs at 315 K. This temperature otherwise called "pseudo-critical temperature" has been subject of several studies in the literature (Hoo-Kyu and Chang-Hyo, 2010; Dang and Hihara, 2010), in which it has been demonstrated that, near the pseudo-critical temperature thermophysical properties of R744 undergo significant changes. Thus, by comparing the results shown in figs. 5a, 6a and 7a, it becomes clear that the pseudo-critical region undergoes a change in position along the gas cooler during the transient period. On the other hand, density, dynamic viscosity and conductivity present a different behavior compared to the specific heat in the pseudo-critical area. Their profiles near the pseudo-critical temperature are characterized by a sharp decrease as shown in figs. 7b, 7c and 7d. However, all R744 thermophysical properties are less sensitive to the change in temperature after the pseudo-critical area.

Fig. 8 shows the transient behavior of Prandtl and Nusselt numbers during the gas cooling process. As can well be observed, tendencies of both numbers are almost identical to the profiles of the specific heat (see Fig. 7a and 7b). Thereby, although properties such as density, dynamic viscosity and thermal conductivity involved in the computation of Prandtl and Nusselt numbers, their influences are insignificant in comparison with the specific heat.

Variation in Prandtl and Nusselt numbers depending on the local temperature of R744 is shown in Fig. 9. The great impact of the specific heat on the Prandtl number is further shown in Fig. 9a, from which it can be seen that the profile is identical to the presented in Fig. 7a. At the pseudo critical temperature, the Prandtl number undergoes sustained growth, which extends to 7 times its nominal value (see Fig. 9a), similarly to the specific heat. The Nusselt number shows a similar trend (see Fig. 9b), but its behavior in the pseudo-critical area is not exactly the same as the specific heat, since it not only depends on the Prandtl number, but also depends on the type of correlation used.

Transient behavior of the local heat transfer coefficient during gas cooling process is shown in Fig. 10. These results are based on the operating conditions such as pressure and mass flux described in Fig. 4 and the Gnielinski (1976) correlation. As can be seen from Fig. 10a, the local heat transfer coefficient of R744 has a significant transient behavior during the gas cooling process. Each profile is characterized by an increase from the input of the gas cooler which grows until reaching a peak value (about 8 times the inlet value) and then decreases in the rest of the process up to the outlet.

Profiles at transient state are characterized by a sharp decline after the maximum magnitude after the peak value in comparison with the profile at steady-state which experienced a large area of constant magnitude after the maximum value. The middle region of gas cooler is characterized by great instability during the transitional period as shown in Fig. 10b). Similar behavior is observed in the specific heat (see Fig. 6b).

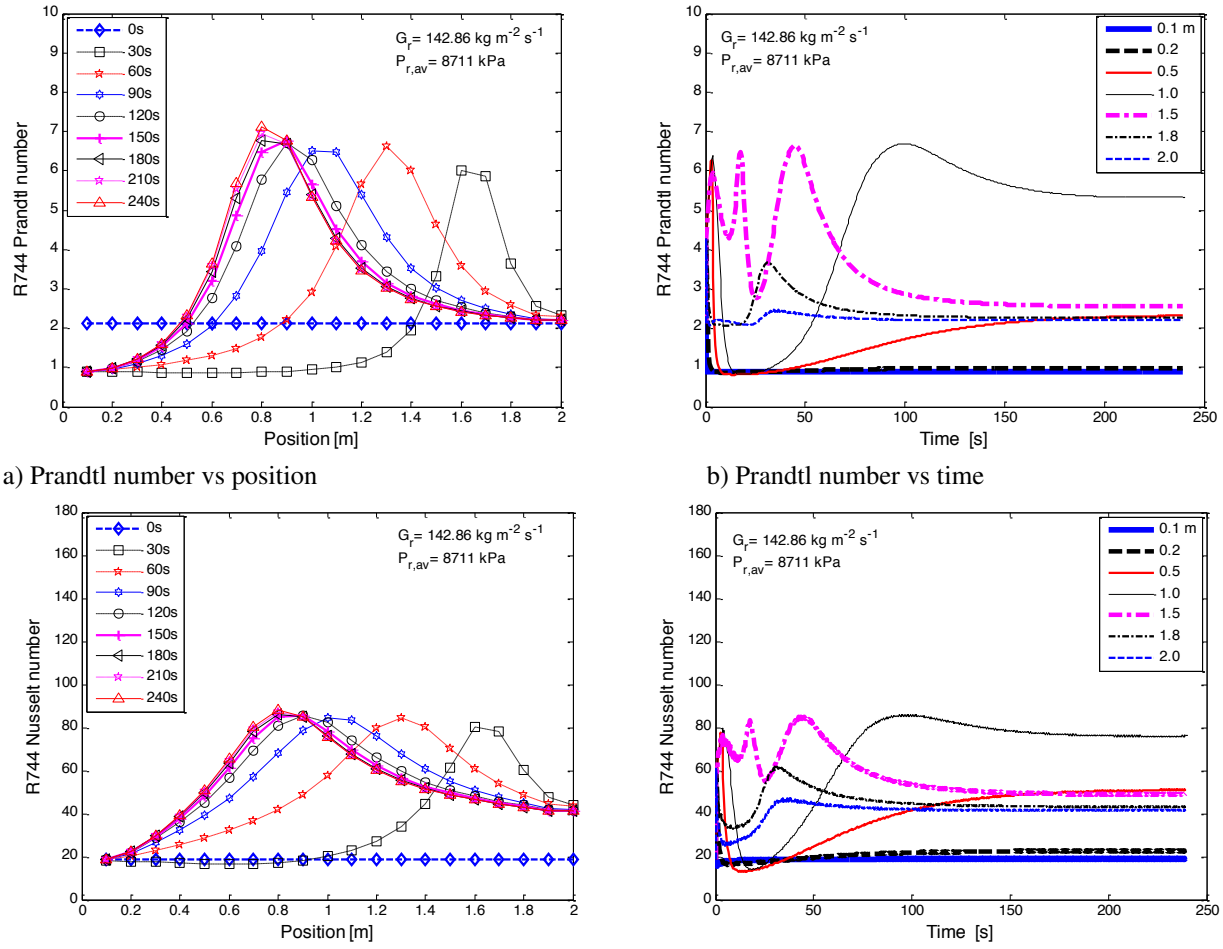

a) Prandtl number vs position

b) Prandtl number vs time

c) Nusselt number vs position

d) Nusselt number vs time

Fig. 8. Transient behavior of the Prandtl and Nusselt numbers along the gas cooler.

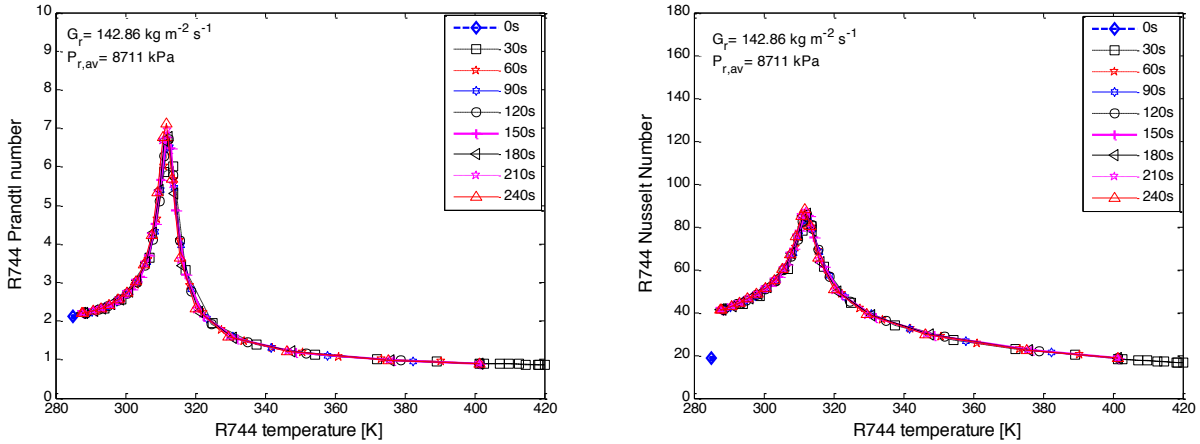

a) Prandtl number

b) Nusselt number

Fig. 9. Behavior of the Prandtl and Nusselt numbers in the supercritical region.

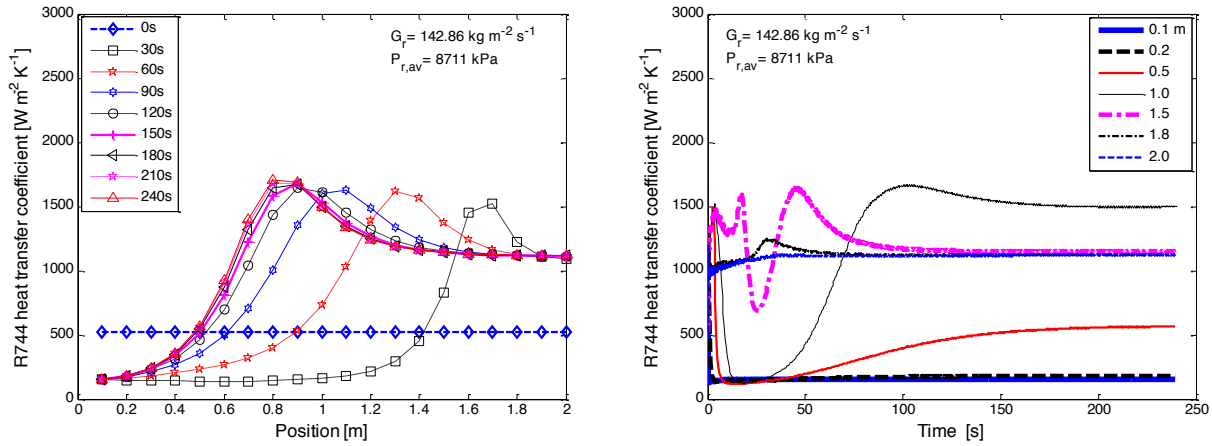

a) Local heat transfer coefficient vs position

b) Local heat transfer coefficient vs time

Fig. 10. Transient behavior of the local heat transfer coefficient along the gas cooler.

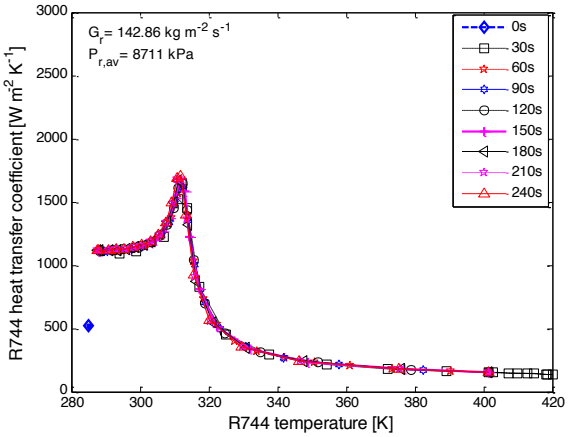

Fig. 11. Transient behavior the local heat transfer coefficient in the supercritical region.

The behavior of the heat transfer coefficient in the supercritical region is shown in Fig. 11. It becomes clear that the peak value that characterizes each profile during the transitional period (see Fig. 10a) corresponds to the pseudo-critical temperature. Therefore, the conclusion reached in the analysis of the specific heat is also valid for the heat transfer coefficient. The analysis from which it is demonstrated that the pseudo-critical area is not at the same location during the transitional period. But undergoes a displacement in the opposite direction to the refrigerant flow until stabilizing at the middle of the gas cooler.

Conclusions

This paper presents comprehensive behavior of R744 thermophysical properties during the startup of gas cooling process in the supercritical region. The study was performed on a horizontal hairpin gas cooler. The model was developed in the Matlab and thermophysical properties were evaluated through the REFPROP dynamic libraries linked to Matlab. The main conclusions are summarized as follows:

- The thermophysical properties of R744 manifest a significant transient behavior during the gas cooling process. This behavior is characterized by large variations in properties along the gas cooler. The area of the curvature of gas cooler is the most affected by transient phenomena.

- The specific heat of R744 is the property most affected by the transient phenomenon in the gas cooler. Its behavior is characterized by an instantaneous change in the amplitude distinguished by a peak value that occurs in the region where the temperature of R744 is pseudo-critical.

- The pseudo-critical area is not at the same location during the transitional period. But undergoes a displacement in the opposite direction to the refrigerant flow until stabilizing at the middle of the gas cooler.

- Local heat transfer coefficient of R744 in the gas cooler as well as Prandtl and Nusselt numbers

behave the same as the specific heat during the transitional period.

- The peak of the local heat transfer coefficient is evaluated at 8 times the ideal value and instantly moves along the gas cooler during the transitional period.

Nomenclature

A	area [m^2]
C	speed of sound [m s^{-1}]
Cp	specific heat [kJ kg^{-1} K^{-1}]
d	tube diameter [mm]
h	specific enthalpy [kJ kg^{-1}]
G	mass flux [kg m^{-2} s^{-1}]
k	thermal conductivity [W m^{-1} K^{-1}]
$\dot{m}$	mass flow [kg s^{-1}]
nz	total number of nodes
P	pressure [kPa]
p	perimeter of inner tubes [m]
T	temperature [K]
t	time [s]
u	velocity [m s^{-1}]
z	axial direction [m]
Greek symbols	
α	convective heat transfer coefficient [W m^{-2} K^{-1}]
ρ	density [kg m^{-3}]
μ	dynamic viscosity [Pa s]
τ_z	shear stress [N m^{-2}]
Δ	increment
Subscripts	
i	inner, cell index
j	cell index
o	outer
r	refrigerant
t	tube
ti	inner tube
sf	secondary fluid
w	water
Superscripts $^\circ$	previous
Superscripts *	guessed
Superscripts ^{s}	staggered

References

Adam-Medina M., Escobar, R.F., Juárez-Romero, D., Guerrero-Ramírez, G.V., López-Zapata, B., (2013). Fault detection in a heat exchanger using second order sliding mode observers. *Revista Mexicana de Ingeniería Química 12*, 327-336.

ASHRAE. (2009). Position Document on Natural Refrigerants, Carbon Dioxide, R744, 4. Available from:http://www2.epa.gov/sites/production/files/documents/ASHRAE_PD_Natural_Refrigerants_2011.pdf

Belman-Flores, J.M. Gallegos-Muñoz, A., Riesco-Ávila, J.M., Zaleta-Aguilar, A., Mendoza-Miranda, J.M., (2014). Exergetic analysis of a refrigeration system. *Revista Mexicana de Ingeniería Química 13*, 957-968.

Björn, P., (2008). Ammonia in low capacity refrigeration and heat pump systems. *International Journal of Refrigeration 31*, 709-715.

Bolaji, B.O., Huan, Z., (2013). Ozone depletion and global warming: Case for the use of natural refrigerant - a review. *Renewable and Sustainable Energy Reviews 18*, 49-54.

Butler, D.J.G., Gigiel, A., Russell, S., (2001). Using air for cooling, Building Research Establishment, *BRE Publication Draft number 202296*.

Cariaga, E., Vergara-Fernandez, A., Levano, M., Vergaray, N., (2013). Numerical simulation of the water saturation at the interface between homogeneous porous medium. *Revista Mexicana de Ingeniería Química 12*, 527-539.

Chen, I.Y., Wang, C.C., Lin, S. Y., (2004). Measurements and correlations of frictional single-phase and two-phase pressure drops of R-410A flow in small U-type return bends. *International Journal of Heat and Mass Transfer 47*, 2241-2249.

Churchill, S.W., (1977). Friction-factor equation spans all fluid flow regimes. *Chemical Engineering Science 7*, 91-92.

Dang, C., Hihara, E., (2010). Numerical study on in tube laminar heat transfer of supercritical fluids. *Applied Thermal Engineering 30*, 1567-1573.

Duffey, R.B., Pioro, I.L., (2005). Experimental heat transfer of supercritical carbon dioxide flowing inside channels (survey). *Nuclear Engineering and Design 235*, 913-924.

Dull, D., Seidel, S., Wells, J., (1989). Moving Forward: Key Implications of the Montreal Protocol. *Studies in Environmental Science 35*, 775-784.

Fang, X., Xu, Y., (2011). Modified heat transfer equation for in-tube supercritical CO_2 cooling. *Applied Thermal Engineering 31*, 3036-3042.

Ge, Y.T., Cropper, R.T., (2009). Simulation and performance evaluation of finned-tube CO2 gas coolers for refrigeration systems. *Applied Thermal Engineering 29*, 957-965.

Gnielinski, V., (1976). New equations for heat and mass transfer in turbulent pipe and channel flow. *Int. Chem. Eng. 16*, 359-68.

Granryd, E., (2001). Hydrocarbons as refrigerants - an overview. *International Journal of Refrigeration 24*, 15-24.

Hoo-Kyu, O., Chang-Hyo, S., (2010). New correlation to predict the heat transfer coefficient in-tube cooling of supercritical CO_2 in horizontal macro-tubes. *Experimental Thermal and Fluid Science 34*, 1230-1241.

Huai, X.L., Koyama, S., Zhao, T.S., (2005). An experimental study of flow and heat transfer of supercritical carbon dioxide in multi-port mini channels under cooling conditions. *Chemical Engineering Science 60*, 3337-3345.

Kim, J.K., Jeon, H.K., Lee, J.S., (2007). Wall temperature measurement and heat transfer correlation of turbulent supercritical carbon dioxide flow in vertical circular/non-circular tubes. *Nuclear Engineering and Design 237*, 1795-1802.

Kim, M.H., Pettersen, J., Bullard, C.W., (2004). Fundamentals process and system design issues in CO_2 vapor compression systems. *Progress in Energy Combustion Science 30*, 119-174.

Lachner, B.F.J., Nellis, G.F., Reindl, D.T., (2007). The commercial feasibility of the use of water vapor as a refrigerant. *International Journal of Refrigeration 30*, 699-708.

Lemmon, E.W., McLinden, M.O., Huber, M.L., (2007). *REFPROP NIST Standard Reference Database 23, v. 8.0*. National Institute of Standards; Gaithersburg, Maryland 20899, USA.

Liao, S.M., Zhao, T.S., (2002). An experimental investigation of convection heat transfer to supercritical carbon dioxide in miniature tubes. *International Journal of Heat and Mass Transfer 45*, 5025-5034.

Li., H., Kruizenga, A., Anderson, M., Corradini, M., Luo, Y., Wang, H., Li, H., (2011). Development of a new forced convection heat transfer correlation for CO_2 in both heating and cooling modes at supercritical pressures. *International Journal of Thermal Sciences 50*, 2430-2442.

Lugo-Leyte, R., Salazar-Pereyra, M., Ruíz-Ramírez, O.A., Zamora-Mata, J.M., Torres-González, E.V. (2013). Exergoeconomic operation cost analysis to theoretical compression refrigeration cycle of HFC-134a. *Revista Mexicana de Ingeniería Química 12*, 361-370.

Neil, A.R., Owen R.C., (2004). Energy saving refrigerant blends comprising R125, R134a, R600 or R600a. *International Refrigeration and Air Conditioning Conference*, 632.

Park, C.Y., Hrnjak, P., (2007). Effect of heat conduction through the fins of a microchannel serpentine gas cooler of transcritical CO_2 system. *International Journal of Refrigeration 30*, 389-397.

Patankar, V., Suhas, (1980). *Numerical heat transfer and fluid flow*. Hemisphere Publishing Corporation. USA.

Peixue, J., Chenru, Z., Jianqiang, D., Wenxing, Z., (2008). Experimental Investigation of Local Heat Transfer of Carbon Dioxide at Super-Critical Pressures in a Vertical Tube and Multi-Port Mini-Channels Under Cooling Conditions. *International Refrigeration and Air Conditioning Conference*, Paper 892.

Pérez-García, V., Belman-Flores, J.M., Navarro-Esbrí, J., Rubio-Maya, C., (2013). Comparative study of transcritical vapor compression configurations using CO_2 as refrigeration mode base on simulation. *Applied Thermal Engineering 51*, 1038-1046.

Petukhov, B.S., Popov,VN., (1963). Theoretical calculation of heat exchanger and frictional resistance in turbulent flow in tubes of incompressible fluid with variable physical properties. *High Temp 1*, 69-83.

Pitla, S.S., Groll, E.A., Ramadhyani, S., (2002). New correlation to predict the heat transfer coefficient during in-tube cooling of turbulent supercritical CO_2. *International Journal of Refrigeration 25*, 887-895.

Rieberer, R., (1999). CO_2 Properties. llR Workshop on CO_2 Technology in Refrigeration. *Heat Pump and Air Conditioning Systems*, Mainz, Germany.

Sánchez, D., Cabello, R., Llopis, R., Torrella, E., (2012). Development and validation of a finite element model for water - CO_2 coaxial gas-coolers. *Applied Energy 93*, 637-647.

Sarkar, J., Agrawal, N., (2010). Performance optimization of transcritical CO_2 cycle with parallel compression economization. *International Journal of Thermal Sciences 49*, 838-843.

Son, C.-H., Park, S.-J., (2006). An experimental study on heat transfer and pressure drop characteristics of carbon dioxide during gas cooling process in a horizontal tube. *International Journal of Refrigeration 29*, 539-546.

Tanaka, K., Higashi, Y., (2010). Thermodynamic properties of HFO-1234yf (2, 3, 3, 3-tetrafluoropropene). *International Journal of Refrigeration 33*, 474-479.

Woerdman, E., (2000). Implementing the Kyoto protocol: why JI and CDM show more promise than international emissions trading. *Energy Policy 28*, 29-38.

Wojtkowiak, J., Popiel, C.O., (2000). Effect of cooling on pressure losses in u-type wavy pipe flow. *International Communications in Heat and Mass Transfer 27*, 169-177.

Yoon-Yeong, B., Hwan-Yeol, K., (2009). Convective heat transfer to CO_2 at a supercritical pressure flowing vertically upward in tubes and an annular channel. *Experimental Thermal and Fluid Science 33*, 329-339.

Yun, R., Hwang, Y., Radermacher, R., (2007). Convective gas cooling heat transfer and pressure drop characteristics of supercritical CO_2/oil mixture in a minichannel tube. *International Journal of Heat and Mass Transfer 50*, 4796-4804.

Zhao, Y., Ohadi, M.O., (2004). Experimental Study of Supercritical CO_2 Gas Cooling in a Microchannel Gas Cooler, ASHRAE.